Biomed Microdevices (2016) 18: 57
DOI 10.1007/s10544-016-0082-y

A novel design for passive misscromixers based on topology optimization method

Xueye Chen[1] · Tiechuan Li[1]

Published online: 20 June 2016

Abstract In this paper, a series of novel passive micromixers, called topological micromixers with reversed flow ($TMRF_X$), are proposed. The reversed flow in the microchannels can enhance chaotic advection and produce better mixing performance. Therefore the maximum of reversed flow is chosen as the objective function of the topology optimization problem. Because the square-wave unit is easier to fabricate and have better mixing performance than many other serpentine micromixers, square-wave structure becomes the original geometry structure. By simulating analysis, the series of $TMRF_X$, namely TMRF, $TMRF_{0.75}$, $TMRF_{0.5}$, $TMRF_{0.25}$, mix better than the square-wave micromixer at various Reynolds numbers (*Re*), but pressure drops of $TMRF_X$ are much higher. Lots of intensive numerical simulations are conducted to prove that TMRF and $TMRF_{0.75}$ have remarkable advantages on mixing over other micromixers at various *Re*. The mixing performance of $TMRF_{0.75}$ is similar to TMRF's. What's more, TMRF have a larger pressure drop than $TMRF_{0.75}$, which means that TMRF have taken more energy than $TMRF_{0.75}$. For a wide range of *Re* ($Re \leq 0.1$ and $Re \geq 10$), $TMRF_{0.75}$ delivers a great performance and the mixing efficiency is greater than 95 %. Even in the range of 0.1–10 for the *Re*, the mixing efficiency of $TMRF_{0.75}$ is higher than 85 %.

Keywords The square-wave micromixer · Topology optimization · The reverse flow · $TMRF_X$ · Numerical simulations

✉ Xueye Chen
xueye_chen@126.com

[1] Faculty of Mechanical Engineering and Automation, Liaoning Univssersity of Technology, Jinzhou 121001, China

1 Introduction

With the rapid development of micro-nano processing technology, machining of micro structures is not a difficulty while structure optimization of the microchannels becomes more and more meaningful (Saatdjian et al. 2012; Chen et al. 2015; Cantu-Perez et al. 2010; Aoki et al. 2011). Among methods of the structure optimization, topology optimization is an important method with characters of freedom, larger design space and superior connectivity (Chen 2016; Zhou et al. 2015). According to different states of the fluid flow, lots of scholars have carried out many meaningful researches on topology optimization including Stokes flow (Aage et al. 2008; Abdelwahed and Hassine 2009; Challis and Guest 2009), Darcy-Stokes flow (Guest and Prévost 2006a; Wiker et al. 2007; Guest and Prévost 2007), Navier–Stokes flows (Evgrafov 2006; Duan et al. 2008; Zhou and Li 2008), unsteady Navier–Stokes flows (Kreissl et al. 2011; Deng et al. 2013), Non-Newtonian flows (Pingen and Maute 2010).

What's more, it is a significant issue how to enhance the mixing of solutions (Lin 2015; Ansari and Kim 2010). Therefore many scholars carried out lots of productive studies on micromixers based on topology optimization (Andreasen et al. 2009; Deng et al. 2012). But due to the addition of convection-diffusion equation, the calculation gets more complex and becomes difficult to convergence. So to reduce the complexity of the calculation, this paper aims at the topology optimization of the square-wave model based on the state of the fluid flow. Due to good mixing performance and simple processing, the square-wave structure has drawn attention of many researcher. A variety of experimental and numerical studies had been carried out for different types of passive micromixers and the results showed that the square-wave microchannel yields the best mixing performance for most Reynolds number (Hossain et al. 2009). What's more, Chen et al. had studied and analyzed species mixing performance of micromixers with serpentine microchannels by numerical simulations in depth and the mixing experiments proved the square-wave serpentine micromixer is flexible, effective, easily fabricated and integrated to a microfluidic system (Chen et al. 2016).

In this paper, based on the reverse flow in microchannels, which has important applications in chemical and biological engineering (Guest and Prévost 2006b), we have proposed a novel numerical model which makes the fluid at the center point of a square-wave structure flow in the opposite direction. By transforming the square-wave structure based on topology optimization of fluid, a novel model was proposed, called the topological micromixer with reversed flow (TMRF). By changing the height of the obstacles in TMRF, three micromixers were created, namely $TMRF_{0.75}$, $TMRF_{0.5}$, $TMRF_{0.25}$. Lots of fruitful numerical simulations were carried out and vast data was analyzed comprehensively in the respects of the concentrations distributions, the velocity field and the pressure drop. At last, we get an outstanding micromixer, $TMRF_{0.75,}$ which delivers a great performance and the mixing efficiency is greater than 95 % for a wide range of *Re* ($Re \geq 5$ or $Re \leq 0.5$).

2 Methodology

2.1 Numerical model

Incompressible Navier–Stokes eqs. Are usually used to describe the dynamic properties of velocity and pressure for incompressible fluidic flows, whose steady form can be expressed as follows (Panton 1984):

$$p(\mathrm{u}\cdot\nabla)\mathrm{u} + \nabla p - \nabla\cdot\eta\left(\nabla \mathrm{u} + (\nabla \mathrm{u})^T\right) = \mathrm{f} \tag{1}$$

$$-\nabla\cdot\mathrm{u} = 0 \tag{2}$$

where **u** is the fluidic velocity, ***p*** is the fluidic pressure, ρ is the fluidic density, η is the fluidic viscosity and f is the body force loaded on the fluid.

In topology optimization of the Navier–Stokes flow, the body force can be expressed as (Borrvall and Petersson 2003)

$$\mathrm{f} = -\alpha \mathrm{u} \tag{3}$$

where α is the impermeability of a porous medium. Its value depends on the optimization design variable γ (Borrvall and Petersson 2003)

$$\alpha(\gamma) = \alpha_{\min} + (\alpha_{\max} - \alpha_{\min})\frac{q(1-\gamma)}{q+\gamma} \tag{4}$$

where $\alpha_{\min}$ and $\alpha_{\max}$ are the minimal and maximal values of α respectively, and q is a real and positive parameter used to adjust the convexity of the interpolation function in Eq. (4). The value of γ can vary between zero and one, where $\gamma = 0$ corresponds to an artificial solid domain and $\gamma = 1$ to a fluidic domain, respectively. Usually, $\alpha_{\min}$ is chosen as 0, and $\alpha_{\max}$is chosen as a finite but high number to ensure the numerical stability of the optimization and to approximate a solid with negligible permeability (Gersborg-Hansen et al. 2005).

In this paper, the geometric model is divided into three parts: the inlet, the design area and the outlet. Among them, the body force f of the inlet and the outlet (non-design area) in the Navier–Stokes eqs. is 0, so f can be defined as follows:

$$\mathrm{f} = \begin{cases} -\alpha \mathrm{u}, & \text{in } \Omega_D \\ 0, & \text{in } \Omega_N \end{cases} \tag{5}$$

Where Ω_D is the design area and Ω_N is the non-design area.

From the above analysis, the model of topological optimization problem can be put forward as follows:

$$\begin{array}{lll} & \min \quad \Phi(u,\gamma) & \\ \text{s.t} & \rho(u\bullet\nabla)u = -\nabla p + \nabla\bullet\eta\left(\nabla u + (\nabla u)^T\right) - \alpha(\gamma)u, & \text{in } \Omega \\ & -\nabla\bullet u = 0, & \text{in } \Omega \\ & \mathrm{u} = u_0, & \text{at } \Gamma_{\text{inlet}} \\ & \mathrm{u} = 0, & \text{at } \Gamma_{\text{wall}} \\ & p = 0, & \\ & \eta\left(\nabla u + \nabla u^T\right)\mathbf{n} = 0 & \text{at } \Gamma_{\text{outlet}} \\ & 0 \leq \gamma \leq 1 & \end{array} \tag{6}$$

Where $\mathbf{u_0}$ is the inlet velocity.

There are two important non-dimensional numbers, namely *Da* and *Re*. *Da* denotes the penetration ability of a porous medium and *Re* represents the ratio of inertia force and viscous force. They are defined as:

$$\mathrm{Da} = \frac{\eta}{\alpha_{\max} \times L^2} \tag{7}$$

$$\mathrm{Re} = \frac{\mathrm{u}L\rho}{\eta} \tag{8}$$

Where *L* indicates the characteristic length of the fluid flow. For non-circular pipes, *L* indicates hydraulic diameter. η indicates coefficient of kinematic viscosity.

Mixing efficiency of the species can be calculated by the formula as follows (Chen et al. 2016):

$$M = 1 - \sqrt{\frac{1}{N}\sum_{i=1}^{N}\left(\frac{c_i - \overline{c}}{\overline{c}}\right)} \tag{9}$$

Where *M* is the mixing efficiency, *N* is the total number of sampling points, c_i and *c* are normalized concentration and expected normalized concentration, respectively. Mixing efficiency ranges from 0 (0 %, not mixing) to 1 (100 %, full mixed).

2.2 Geometrical model

Hossain et al. have conducted a computational fluid dynamic investigation of mixing performance for three different microchannels, i.e., a zigzag, square-wave and curved channels in 2009 (Hossain et al. 2009) and Chen et al. have studied and analyzed species mixing performance of micromixers with serpentine microchannels by numerical simulations and experiments in depth in 2016 (Chen et al. 2016). All above papers proved that the square-wave micromixer has advantages over other micromixers with serpentine microchannels on mixing performance for most Reynolds numbers. Therefore the square-wave structure was chose as the original structure for optimization. Figure 1 shows the sizes and structure in details.

Figure 1 gives the schematic diagram of the original structure. To the contrast of Hossain's model, the sizes in Fig. 1 were designed by reference to the paper (Olesen et al. 2004). The middle part (depicted in yellow) acted as the design area and the rest acted as the non-design area. The unit of sizes is mm.

2.3 Analysing and solving

For the solution of the optimization problem, the finite element analysis (FEA) software COMSOL 4.4 integrates many useful physical modules, which can be smoothly coupled. In this model, laminar flow module and optimization and sensitivity analysis module were used for the topology optimization problem. The discrete adjoint sensitivity method was integrated in optimization and sensitivity analysis module, so it is not need other software for application development to solve the sensitivity analysis in Fig. 2.

For the sensitivity analysis of the optimization problem in (6), we use the adjoint sensitivity method which can

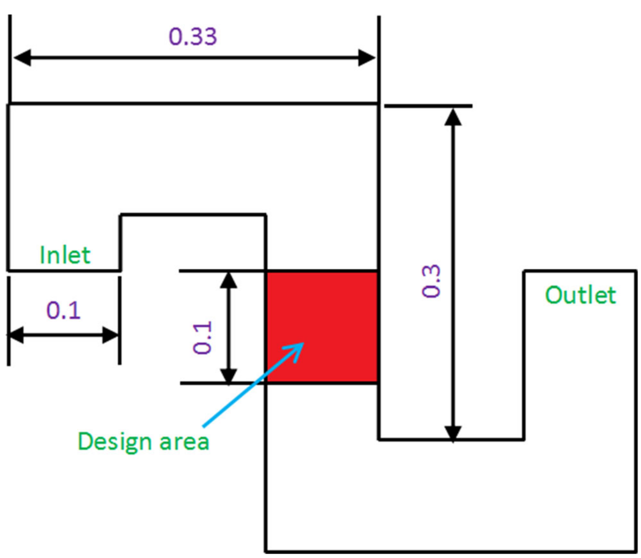

Fig. 1 Schematic diagram of the original structure

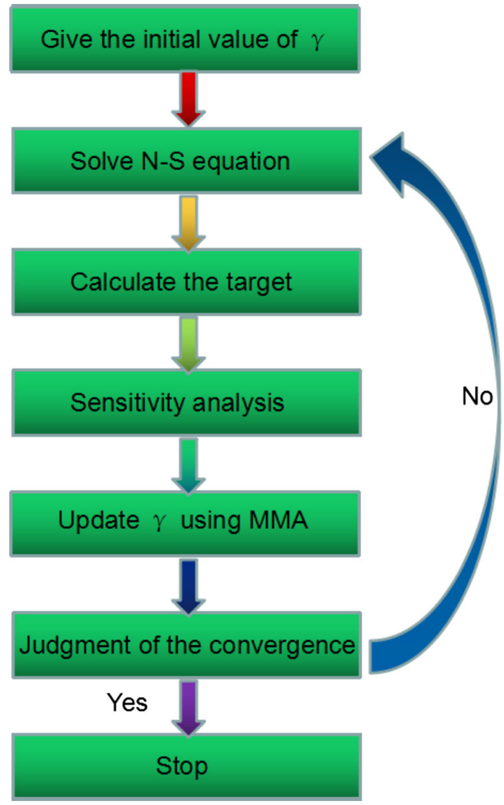

Fig. 2 Optimization flow chart

effectively evaluate sensitivity. The sensitivity problem can be written using the chain rule as that of finding:

$$\frac{d}{d\xi}Q(u(\xi),\xi)=\frac{\partial Q}{\partial \xi}+\frac{\partial Q}{\partial u}\cdot\frac{\partial u}{\partial L}\cdot\frac{\partial L}{\partial \xi} \tag{10}$$

where, $Q(\xi)$is scalar-valued objective function, $\xi$is the control variables, u is the solution variables and$L(u(\xi),\xi)=0$is a system of equations of the discretization PDE. The first term$\partial Q/\partial u$, which is an explicit partial derivative of the objective function with respect to the control variables is easy to

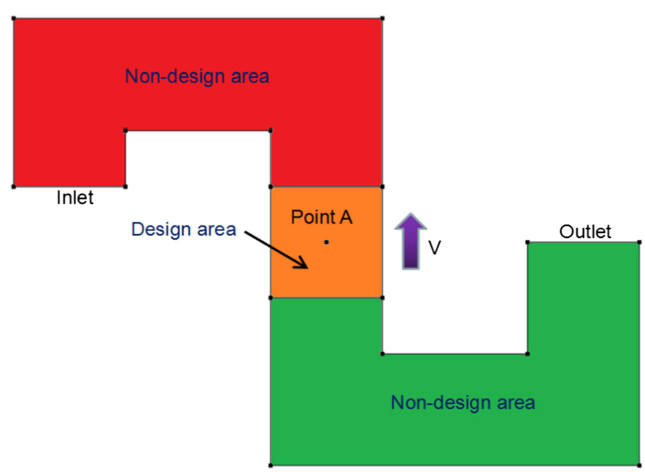

Fig. 3 Schematic diagram of the reversed flow model

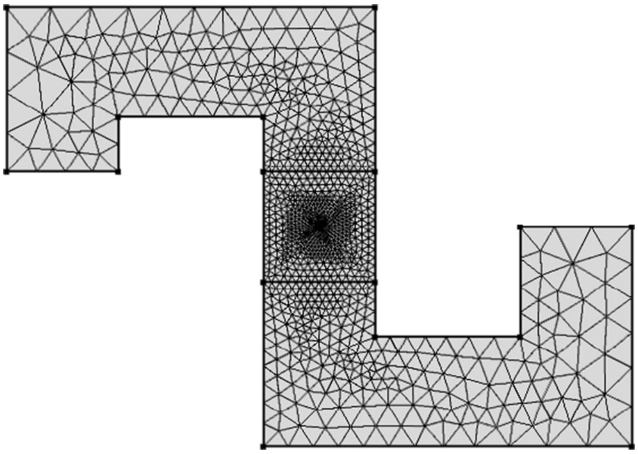

Fig. 4 Schematic diagram of the mesh division of the topology model

compute using symbolic differentiation. The second term is more difficult to deal with. The first and last factors, $\partial Q/\partial u$-and$\partial l/\partial \xi$can be computed directly using symbolic differentiation. The key to evaluating the complete expression lies in noting that the middle factor can be computed as $\partial u/\partial L = (\partial L/\partial u)^{-1}$ and that $\partial L/\partial u$ is the PDE Jacobian at the solution point:

$$\frac{d}{d\xi}Q(u(\xi),\xi) = \frac{\partial Q}{\partial \xi} + \frac{\partial Q}{\partial u}\cdot\left(\frac{\partial L}{\partial u}\right)^{-1}\cdot\frac{\partial L}{\partial \xi} \tag{11}$$

Evaluating the inverse of the N-by-N Jacobian matrix is too expensive. In order to avoid that step, an auxiliary linear problem can be introduced. This can be done with the adjoint sensitivity method.

Introduce instead the N-by-1 adjoint solution u*, which is defined as:

$$u^* = \frac{\partial Q}{\partial u}\cdot\left(\frac{\partial L}{\partial u}\right)^{-1} \tag{12}$$

Multiplying this relation from the right with the PDE Jacobian$\partial L/\partial u$and transposing leads to a single linear system of equations:

$$\frac{\partial L^T}{\partial u}\cdot u^* = \frac{\partial Q}{\partial u} \tag{13}$$

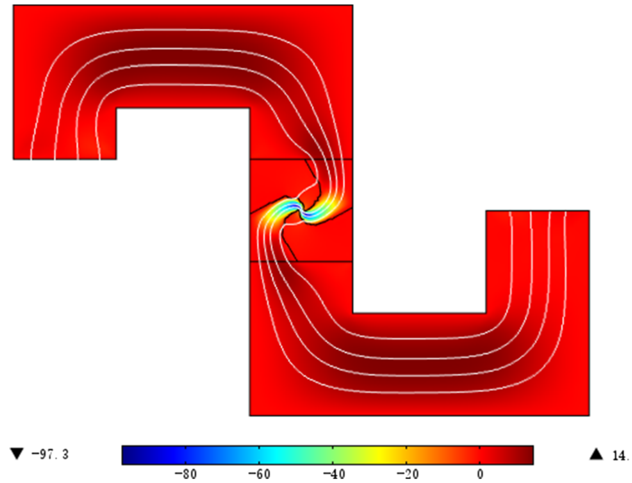

Fig. 6 The velocity field (streamlines) after optimization

In Fig. 2, the optimization algorithm is important to update the design variable γ in the optimization flow chart. The method of moving asymptotes (MMA) was proved applicable for our model (single objective nonlinear programming problem) (Svanberg 1987), which was integrated smoothly in the optimization solver of COMSOL 4.4.

3 Results and discussion

In order to reduce the complexity of the calculation, this paper aims at the topology optimization of the square-wave model based on the fluid flow state. That is, material transfer is not involved in the topology optimization problem. In this work, two steps need to be completed, i.e., achieve the optimal topology configuration using topology optimization method and discuss the mixing performance of the topological structure micromixer.

3.1 Result of the topology optimization

In this topology optimization problem, in order to form the reversed flow at the center of the design area, function -v was chose as the objective in Eq.(6). That is, the maximum of v (longitudinal velocity) is the optimal result.

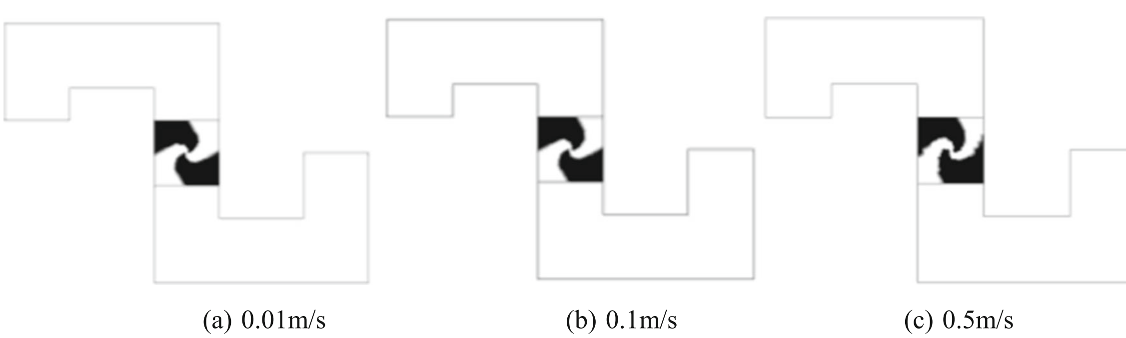

Fig. 5 Schematic diagrams of the topology models with different inlet velocities

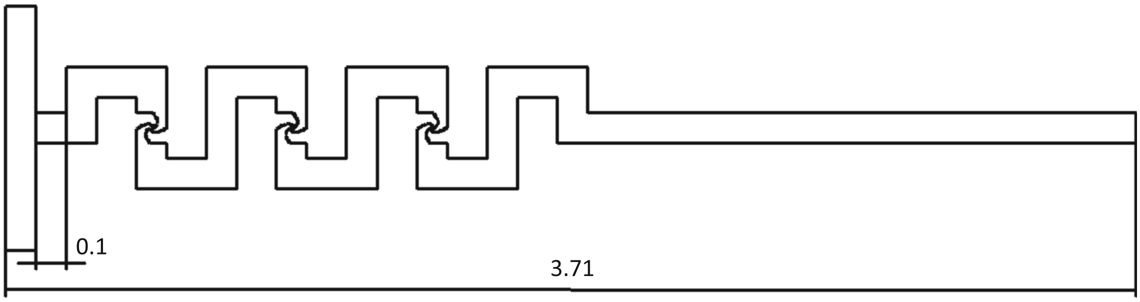

Fig. 7 Schematic diagram of the topological micromixer

The center point A of the design area was chose as the optimization objective point and the direction of v was defined in Fig. 3 clearly. It proved that the way to select the objective function conforms to minimizing the power dissipation inside the fluidic domain (Olesen et al. 2004). Of course the reversed flow increases the contact area between the mixing solutions and improve the mixing performance. The detail discussion about the topological model has been elaborated in the next section.

The convergence of the optimization process depends on three important factors: the Darcy number, the mesh size and the coefficient q. Through calculation and adjustment, parameter settings are as follows:

Topology optimization parameter settings

Da	α_{min}	*L*	*q*
10^{-5}	0	0.1	1

In this model, the mesh type was free triangular and the number was 1923 (see Fig. 4).

Based on different inlet velocities, namely 0.01 m/s, 0.1 m/s and 0.5 m/s, three topological models were obtained showed in Fig. 5.

Figure 5 gives sketches of the topology models with different inlet velocities. Seen from the figure, the inlet velocity of the topological model has little effect on the structure. Seen from Fig. 5(c), the boundary of the solid obstruction (the black parts) with 0.5 m/s was less smooth than the other two models. Larger velocity made numerical oscillations disturb the FEM program. Therefore the model with inlet velocity at 0.01 m/s is appropriate for the topological structure.

Figure 6 shows the velocity field after optimization described by streamlines. The plots revealed how the flow turns around, with a negative velocity at the center of the channel. The velocity has a minimum of roughly −0.15 m/s at the design point.

3.2 Discussion about $TMRF_X$

Using image processing techniques, the topological model based on reversed flow was extracted. Expanding the

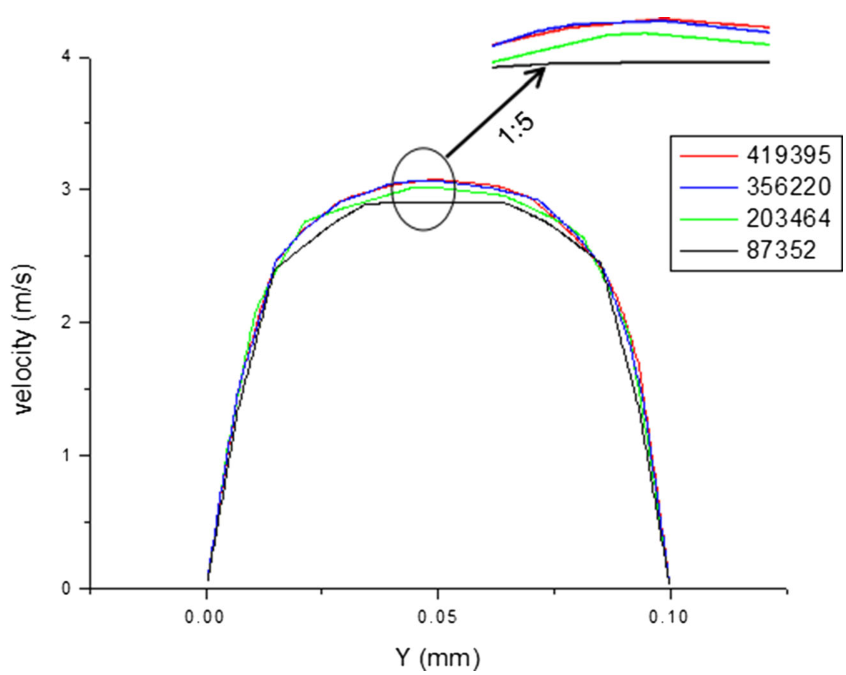

Fig. 8 The local velocity profiles along the middle line at the outlet at $Re = 100$

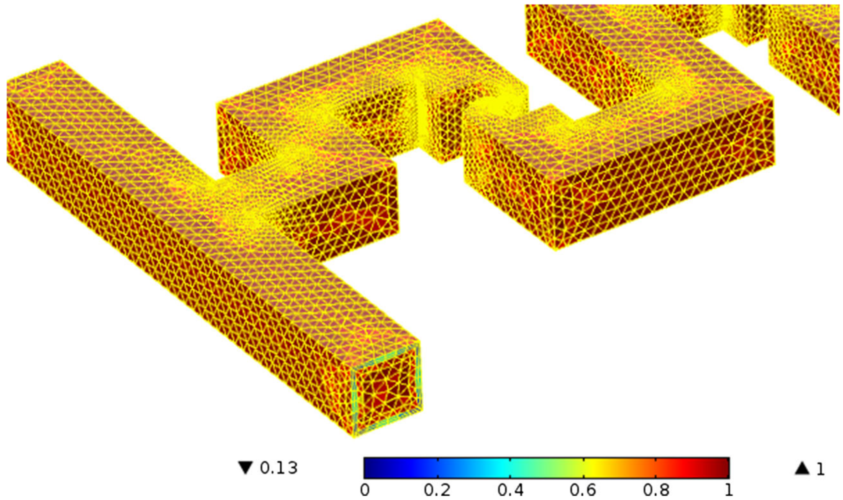

Fig. 9 The mesh system of TMRF with 356,220 elements

structure, the square-wave micromixer was transformed as shown in Fig. 7, in which the unit of the new micromixer sizes is mm.

A novel model was proposed as shown in Fig. 7, called the topological micromixer with reversed flow (TMRF). The width of the channel in TMRF is 0.1 mm as shown in Fig. 1 and the height is 0.1 mm as well.

Two main physical models, namely laminar flow and transport of diluted species, were used in simulations by COMSOL 4.4. The results of simulations of the square-wave micromixer were effective and have been proved to be accurate by our paper (Chen et al. 2016) which was published in 2016. For comparison purposes, the dynamic viscosity, density and the diffusion coefficient were 10^3kg·s/m, 10^3kg/m3, and 10^{-9} m^2/s, respectively.

It is significant to verify the grid-independent of the solutions. Therefore in order to find out the optimal number of grids, four structured grid systems, wherein the number of grids ranged from 87,352 to 419,395, were tested for each microchannel. Finally, 356,220 was chose from the results of the grid-dependency test as the optimal number of grids. Figure 8 shows the local velocity profiles along the middle line at the outlet at $Re = 100$ with four mesh refinements. Seen from the figure, 356,220 is the minimum of the elements for meshing the TMRF model to obtain a mesh-independent solution.

A good mesh system is important for improving the accuracy of simulation and saving time of calculation. Correspond to Figs. 8 and 9 shows mesh system of TMRF with 356,220 elements.

In Fig. 9, the color legend represented the quality of elements. It showed that the minimum element quality can reach as high as 0.13 and through statistics by COMSOL 4.4 the average element was as high as 0.58. According to FEM theory, it is enough accurate and effective to solve and analyze the TMRF.

Based on the structure of TMRF, several structures were derived. Figure 10 shows the derivatives from TMRF.

Seen from Fig. 10, different structures were produced by changing the ratio of the height of obstacles (h) to the height of

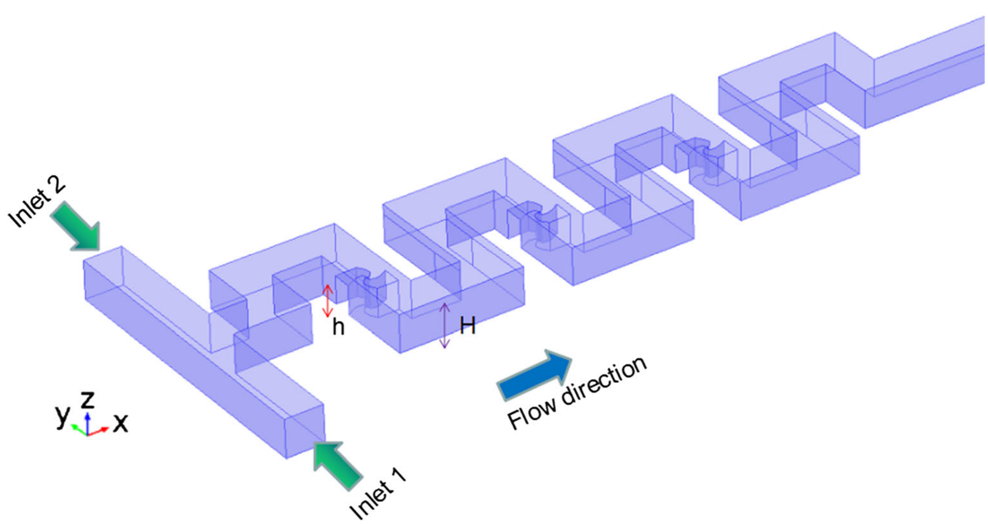

Fig. 10 Schematic diagrams of $TMRF_X$

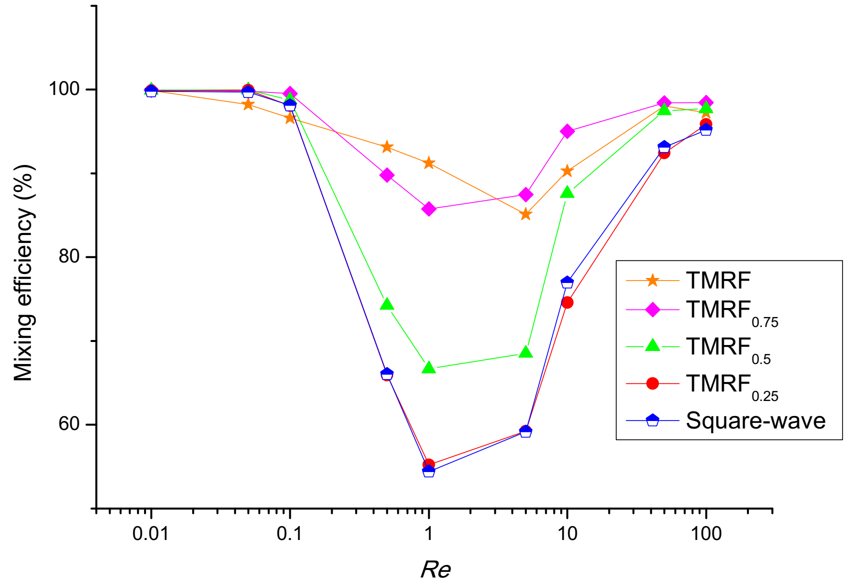

Fig. 11 Variations of the mixing efficiency with different *Re* at the exit of the micromixers

the microchannel (H). Except for 1 (TMRF), 0.75, 0.5, 0.25 and 0 were chosen as the values of h/H, namely $TMRF_{0.75}$, $TMRF_{0.5}$, $TMRF_{0.25}$, the square-wave micromixer respectively.

On the basis of Fig. 10, five micromixers were simulated under different *Re*. Figure 11 shows variations of the mixing efficiency with different *Re* at the exit of the micromixers.

As shown in Fig. 11, the series of $TMRF_X$ had an advantage over the square-wave micromixer on mixing performance with different *Re*, especially micromixers with X (h/H) of $TMRF_X$ beyond 0.25. When *Re* was less than 0.1 or more than 50, five micromixers have similar mixing performance, all beyond 90 %, due to the numeric limit of 100 %, which the mixing efficiency will never reach. But during *Re* being between 0.1 to 50, the mixing efficiency strengthened obviously with X (h/H) increasing.

Seen from Fig. 11, two cases should be discussed, the case at low *Re* and the case at high *Re*. Figure 12 showed the mixing performance of the micromixers with low *Re*, namely 0.05, 0.5. Seen from the structures, it is easy to know the Fig. 12(a), (b), (c), (d) and (e) represent TMRF, $TMRF_{0.75}$, $TMRF_{0.5}$, $TMRF_{0.25}$ and the square-wave micromixer. In Fig. 12, the colour of the streamlines and planes in the micromixers denoted the concentration distribution.

At low *Re*, the mixing is limited by molecular diffusion and the mechanical stirring is ineffective at $Re << 1$ (Olesen et al. 2004). When *Re* is low, the intensity of molecular diffusion becomes weaker with *Re* increasing. Therefore the mixing efficiency of each micromixers went down with *Re* increasing. But the rate of decline of mixing efficiency is different with various structures. At a *Re* of 0.05, the molecular diffusion is strong and each micromixers can obtain good mixing performance. But as can be seen from the streamlines in Fig. 12, laminar flow is the main flow state at a *Re* of 0.5. So at $Re = 0.5$, the mixing performance of the micromixers is bad. Because of the reversed flow structure, the mixing efficiency of $TMRF_X$, especially TMRF and $TMRF_{0.75}$, fall off more slowly than the square-wave micromixer's. The mixing at low *Re* is dominated by the residence time and depends on the total path of the flow (Gersborg-Hansen et al. 2005). The reversed flow structure happened to increase the total path of the flow and the residence time was prolonged due to the reversed turn. Seen from Figs. 11 and 12, the mixing efficiency went up with the X (h/H) of $TMRF_X$ increasing. Therefore the TMRF and $TMRF_{0.75}$ have a remarkable advantage on mixing over other micromixers at low *Re*.

Seen from Fig. 11, when $Re \geq 1$, the mixing performance of each micromixer was better with *Re* increasing. Because when $Re > 1$, convection dominates gradually the mix with the increase of *Re*. What's more, the intensity of convection depends on *Re*. It is obvious that TMRF and $TMRF_{0.75}$ still have best mixing performance among five micromixers at higher *Re* by reference to Fig. 11. Velocity-vector plots on planes of five micromixers at *Re* of 5, 10, 50 and 100 were shown in Figs. 13, 14, 15, 16 and 17 especially.

At a *Re* of 5, the streamlines and planes of each micromixers were shown in Fig. (a) of Figs. 13-17. The colour of the streamlines and planes in the micromixers denoted the concentration distribution. By reference to Fig. 11, mixing of each micromixer was at a low ebb, because convection and molecular diffusion are both weak and laminar flow shows obviously. But the reversed turn in $TMRF_X$ made part of fluid slow even reverse, which increased contact area between two solutions. From Figs. 13-17, although the intensity of convection and molecular diffusion became weak, the reversed turn still improve the mixing efficiency beyond 85 % in TMRF and $TMRF_{0.75}$.

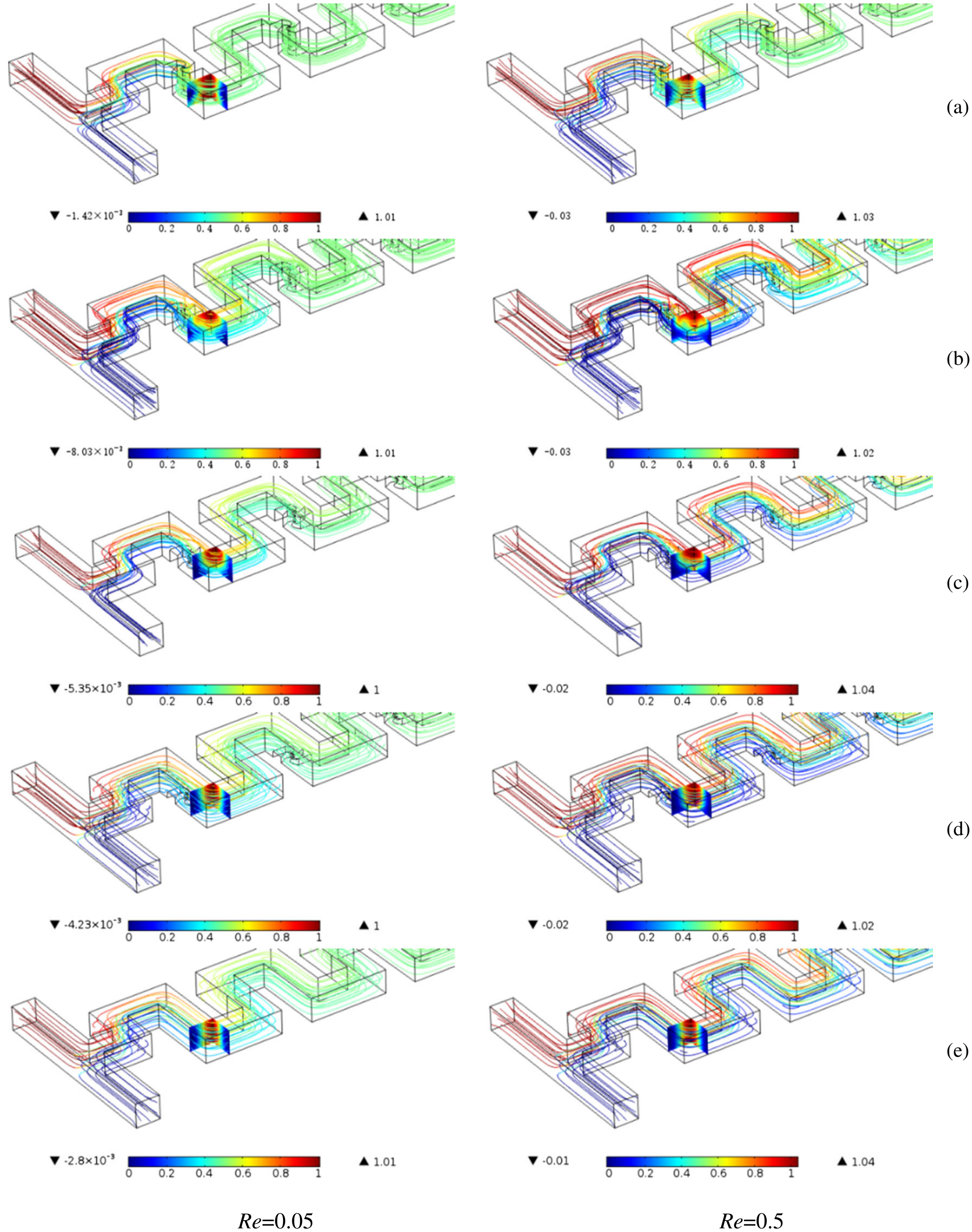

Fig. 12 Mixing performance of five micromixers at *Re* = 0.05 and *Re* = 0.5: (**a**)TMRF (**b**)$TMRF_{0.75}$ (**c**)$TMRF_{0.5}$ (**d**)$TMRF_{0.25}$ (**e**)Square-wave

With *Re* increasing, laminar flow was gradually broken in each micromixer. It is a meaningful principle that a high *Re* can encourage an adverse pressure gradient and vortical flow, which produces secondary flow to enhance mixing. When the fluid flow through the turning, the solutions near the inner corner speeds up and the solutions near the outer corner slows down. So the structure at the turn affects the intensity of vortex and the mixing performance at high *Re*. Contrasting Fig. 13 with Fig. 17, the regular vortex was formed in TMRF at a *Re* of 10 but in the square-wave micromixer at a *Re* of 50. It is easy to draw the conclusion the reversed turn indeed enhances the

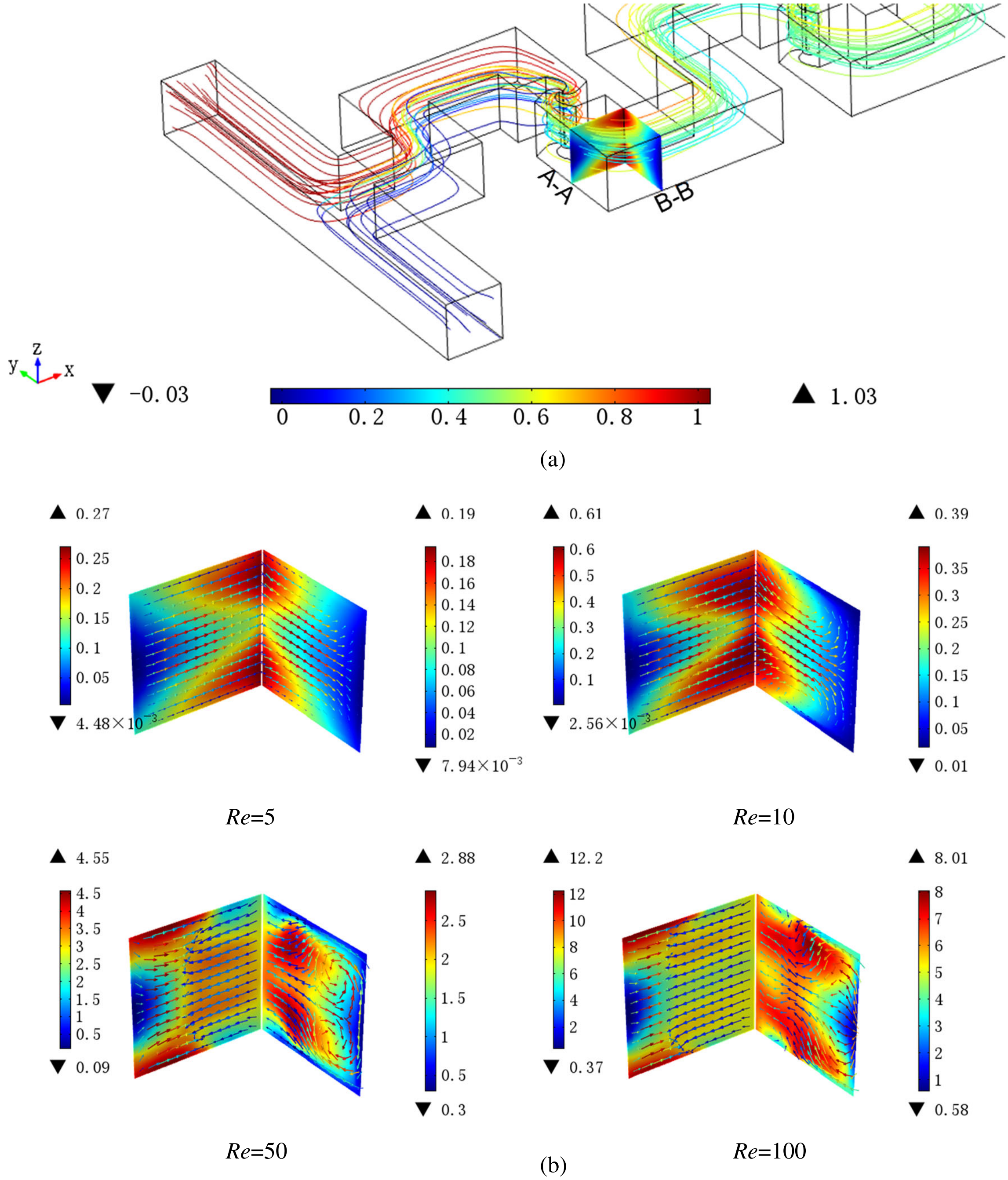

Fig. 13 Velocity-vector plots on planes of TMRF

centrifugal force at the turn and produces secondary flow to enhance mixing. Seen from velocity-vector plots on planes of two micromixers at various *Re*, the intensity of the secondary flow of TMRF was stronger than the square-wave micromixer's at each *Re*.

Contrasting $TMRF_X$, it is interesting to find that the mixing efficiency of $TMRF_{0.75}$ was better than TMRF's at *Re* beyond 5. Seen from velocity-vector plots in Figs. 13 and 14, it is easy to know a counterclockwise vertex was formed at plane A-A of $TMRF_{0.75}$. Because the obstacle in $TMRF_{0.75}$ was not in direct contact with the upper surface of $TMRF_{0.75}$ and some fluid rushed through the space left behind. The other fluid flowed along the reversed turn and joined the fluid over the reversed turn. Therefore the vortex formed on account of centrifugal force. Although two vortexes in plane B-B of $TMRF_{0.75}$ became asymmetry, the mixing efficiency of $TMRF_{0.75}$ was better than TMRF's at high *Re* by reference to Fig. 11. It is easy to know that vortex formed two times enhanced mixing. But the height of the obstacle was

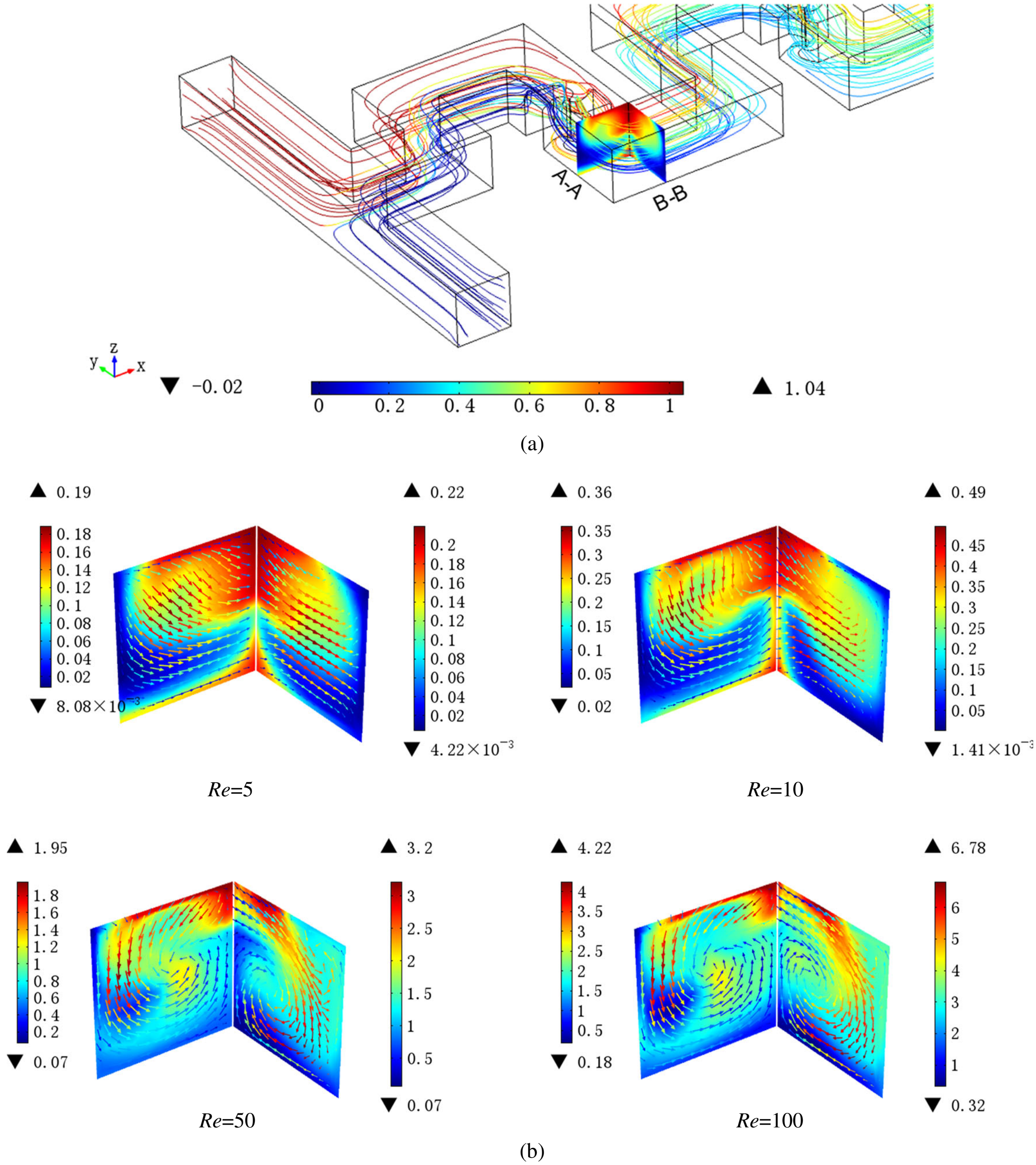

Fig. 14 Velocity-vector plots on planes of $TMRF_{0.75}$

small, especially below the half of the channel height, the intensity of vortexes in plane A-A and plane B-B was weak by contrasting Fig. 13 with Fig. 16. In conclusion, TMRF and $TMRF_{0.75}$ still have an advantage on mixing over other micromixers at high *Re*.

Figure 18 shows the contrast curves of the pressure drops of five micromixers at various *Re*. In all cases, the pressure drops were calculated by processing the pressure datum of inlet and outlet of the micromixers.

It is meaningful to study the pressure drop which is directly related to the input energy used for the mixing. Duo to the reversed turn in the $TMRF_X$, the pressure drop increases more rapidly than the square-wave micromixer at each *Re*. When solutions flowed through the obstacle, some fluid was forced to from adverse current. Seen from Fig. 18, the pressure drop enhances with the increasing of X (h/H) at each *Re*. Because the increasing of the obstacle height produced a hindering function for the fluid. By reference to Figs. 18 and 11, it is easy to know the mixing performance of TMRF and $TMRF_{0.75}$ were similar and they were the best mixing performance among five micromixers at all *Re*. But TMRF had larger pressure drop than $TMRF_{0.75}$. That is TMRF had taken more energy than $TMRF_{0.75}$.

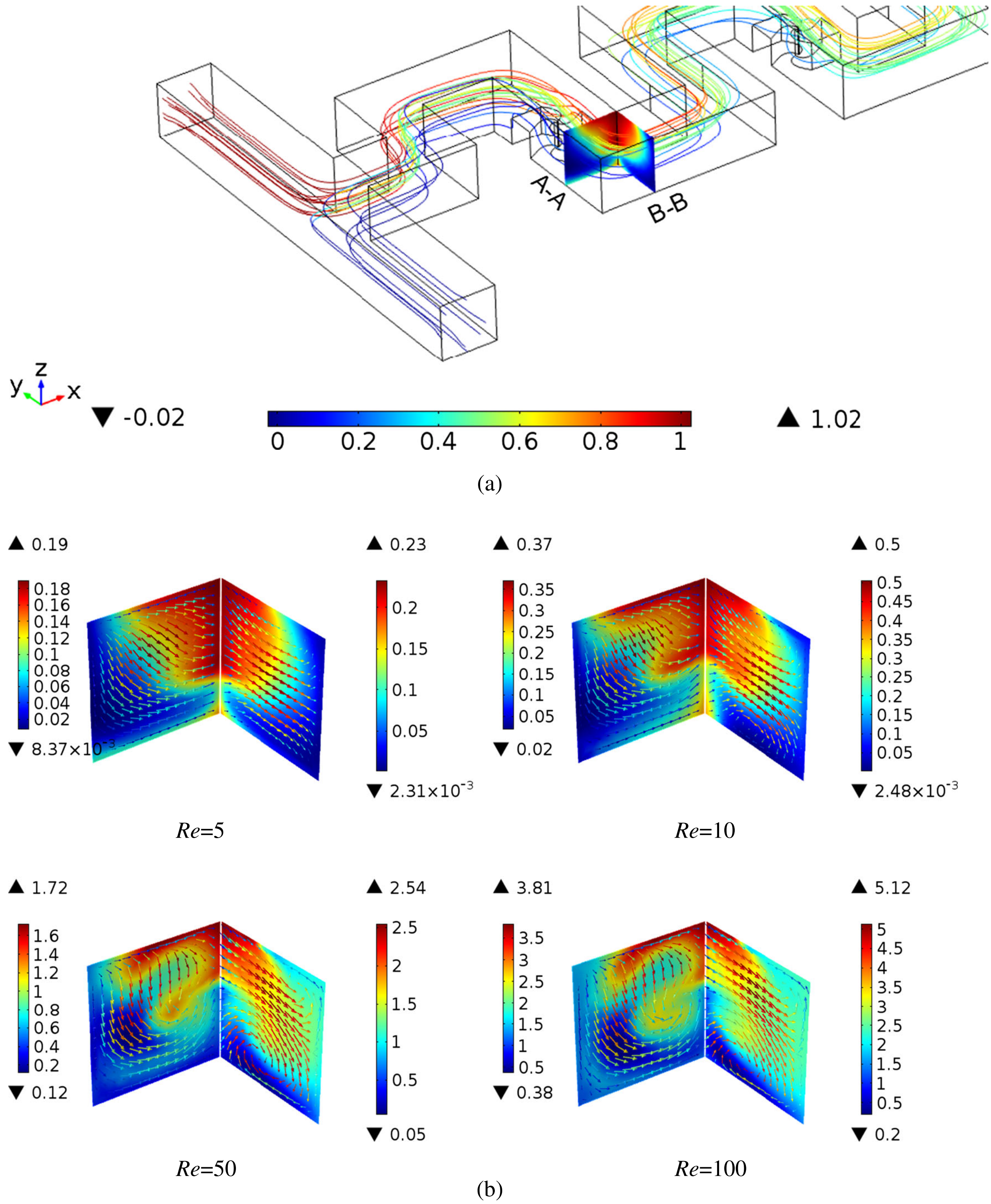

Fig. 15 Velocity-vector plots on planes of $TMRF_{0.5}$

Figure 19 shows the concentration distribution of unit planes of $TMRF_{0.75}$ and TMRF at *Re* of 0.1, 5 and 10. It is easy to understand that convection and molecular diffusion dominated species mixing with the increase of *Re*. It is also easy to know two micromixers had a similar mixing performance at each *Re*. Therefore by comparing the pressure drop of two micromixers, $TMRF_{0.75}$ have more advantages as an outstanding micromixer.

4 Conclusions

In this paper, we proposed a novel design for passive micromixers based on topology optimization method and the topological micromixer with reversed flow (TMRF). By changing the height of the obstacles in TMRF, three micromixers, namely $TMRF_{0.75}$, $TMRF_{0.5}$, $TMRF_{0.25}$, were added to contrast with TMRF and the square-wave

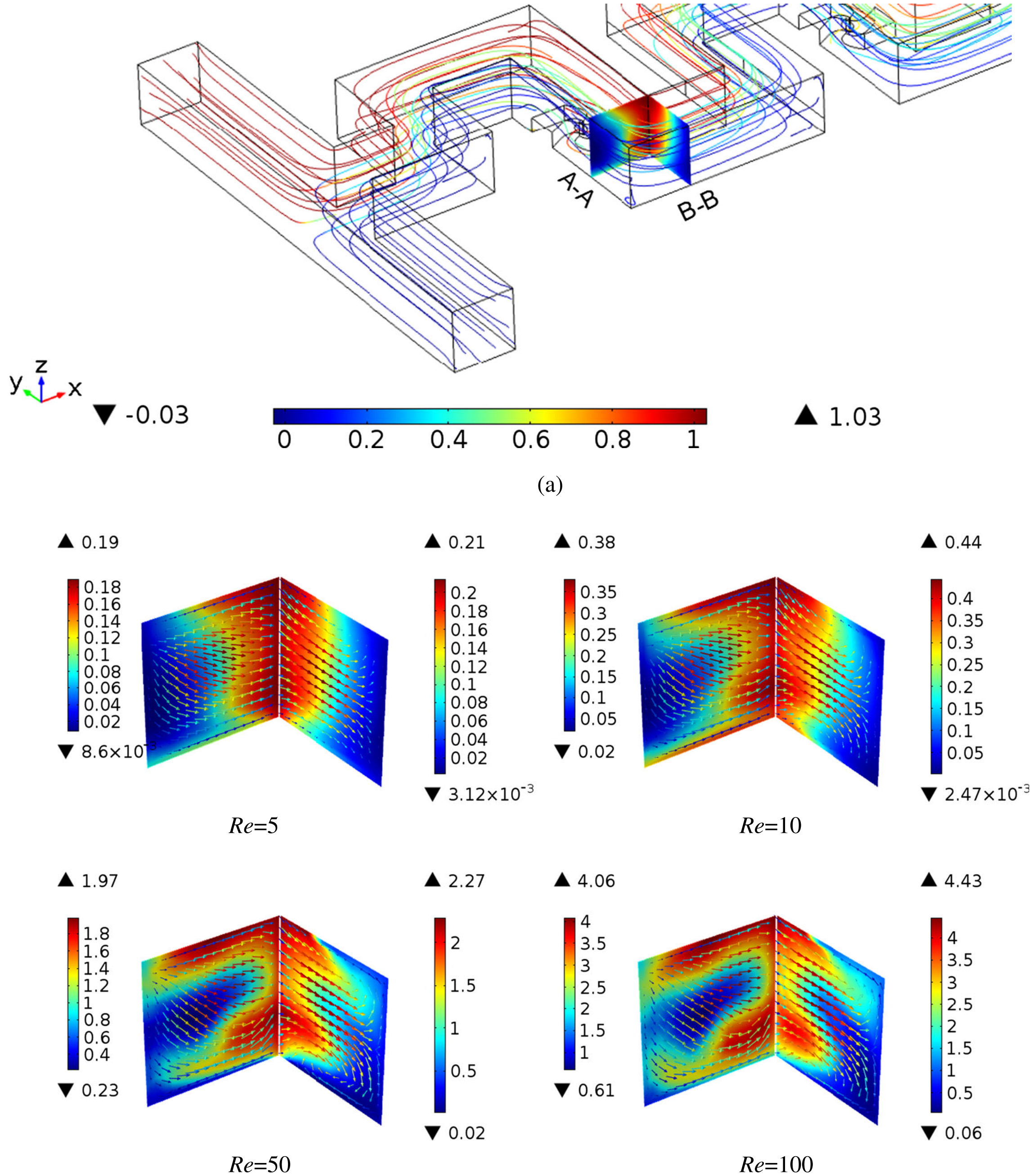

Fig. 16 Velocity-vector plots on planes of $TMRF_{0.25}$

micromixer. Lots of intensive numerical simulations were conducted to evaluate the performance of five micromixers, namely TMRF, $TMRF_{0.75}$, $TMRF_{0.5}$, $TMRF_{0.25}$, the square-wave micromixer. By comparing the performance of five micromixers, some significative conclusions can be drawn as follows:

(i) With the development of advanced manufacture technology, structure design method of microfluidic chips is particularly important. On account of rapid development of micro-nano processing technology, such as the mature of 3D printing, it is not a difficulty to fabricate the complex structure designed by topology optimization method of fluid, which has contributed to a universal guide on how to make the solutions mix efficiently. The contrast of $TMRF_X$ with the square-wave micromixer can prove that the reverse flow model designed based on topology optimization enhanced the mixing efficiency of two solutions observably. At a *Re* of 10, the mixing efficiency of TMRF at outlet was 91.2 %, but the square-wave

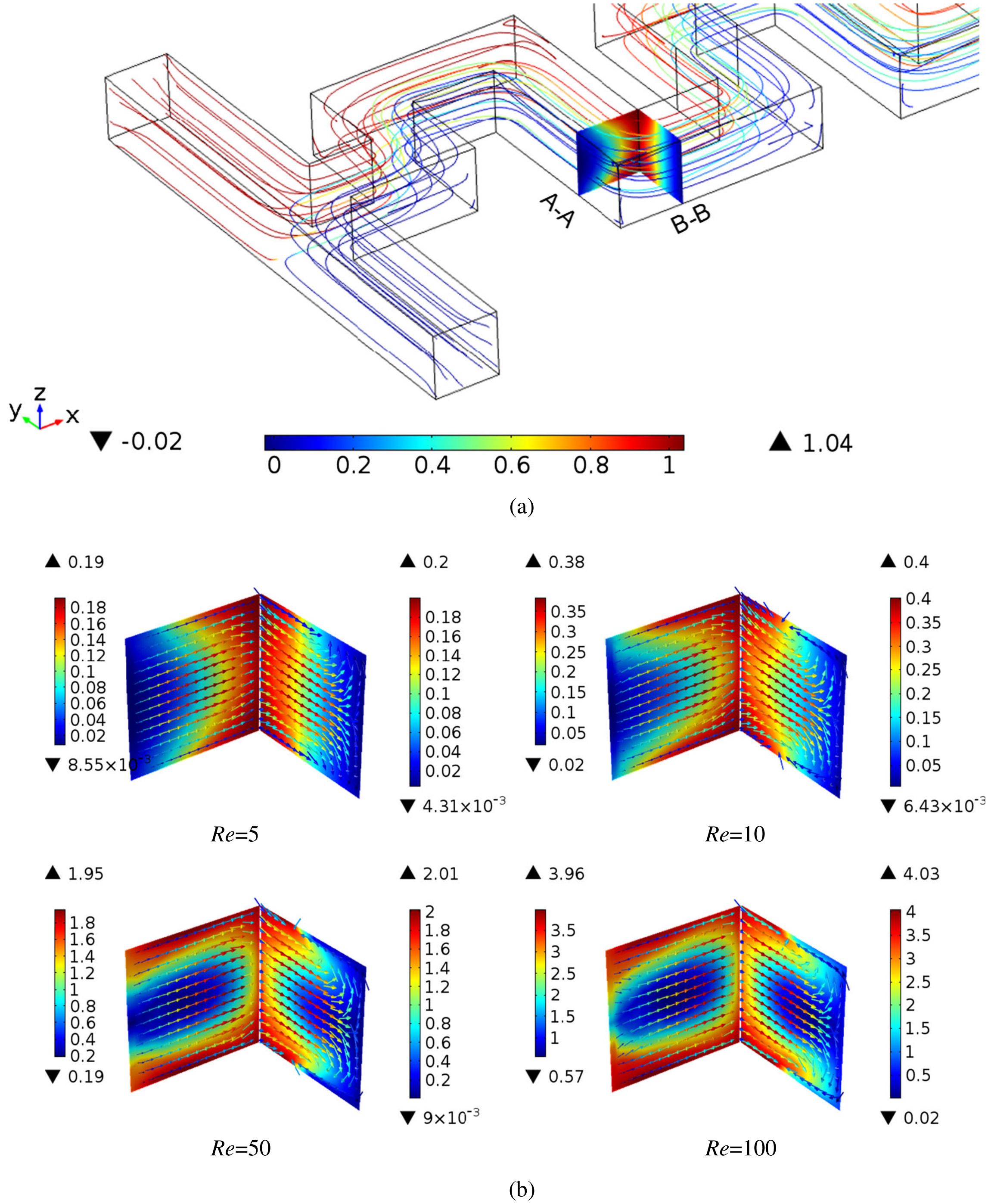

Fig. 17 Velocity-vector plots on planes of the square-wave micromixer

micromixer's was only 54.4 %. Therefore the method is significant and has potential value.

(ii) At low *Re*, the mixing is limited by molecular diffusion and the intensity of molecular diffusion becomes weaker with *Re* increasing. But the mixing efficiency of $TMRF_X$, especially TMRF and $TMRF_{0.75}$, fall off more slowly than the square-wave micromixer's due to the reversed flow structure, which happened to increase the total path of the flow and the residence time was prolonged. It was interesting that the mixing efficiency went up with the X (h/H) of $TMRF_X$ increasing. Therefore TMRF and $TMRF_{0.75}$ have a remarkable advantage on mixing over other micromixers at low *Re*.

(iii) At high *Re*, laminar flow was gradually broken in each micromixer with *Re* increasing and the high *Re* can encourage an adverse pressure gradient and vortical flow, which made secondary flow to enhance mixing. The regular vortex was formed in TMRF at a *Re* of 10 but

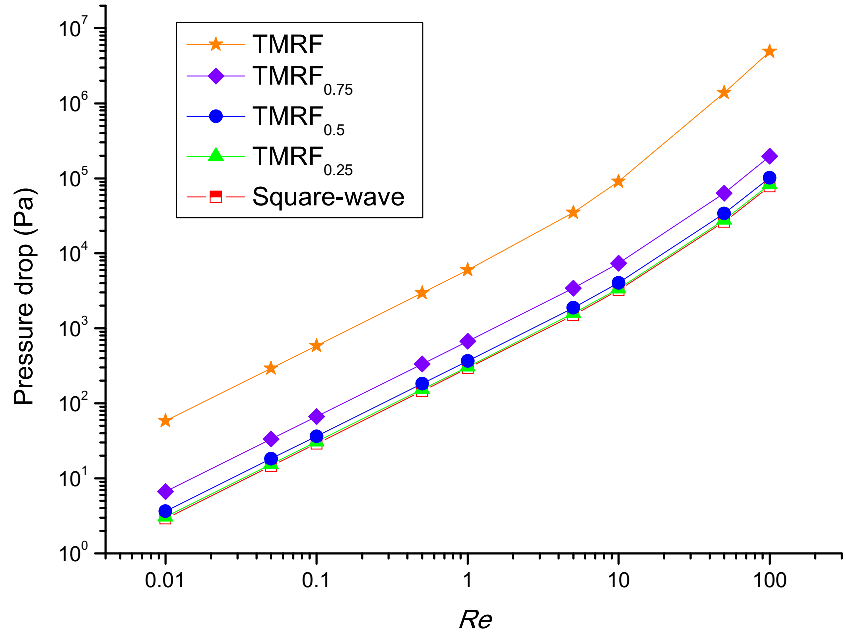

Fig. 18 Variation of the pressure drop with different *Re* for the different geometries

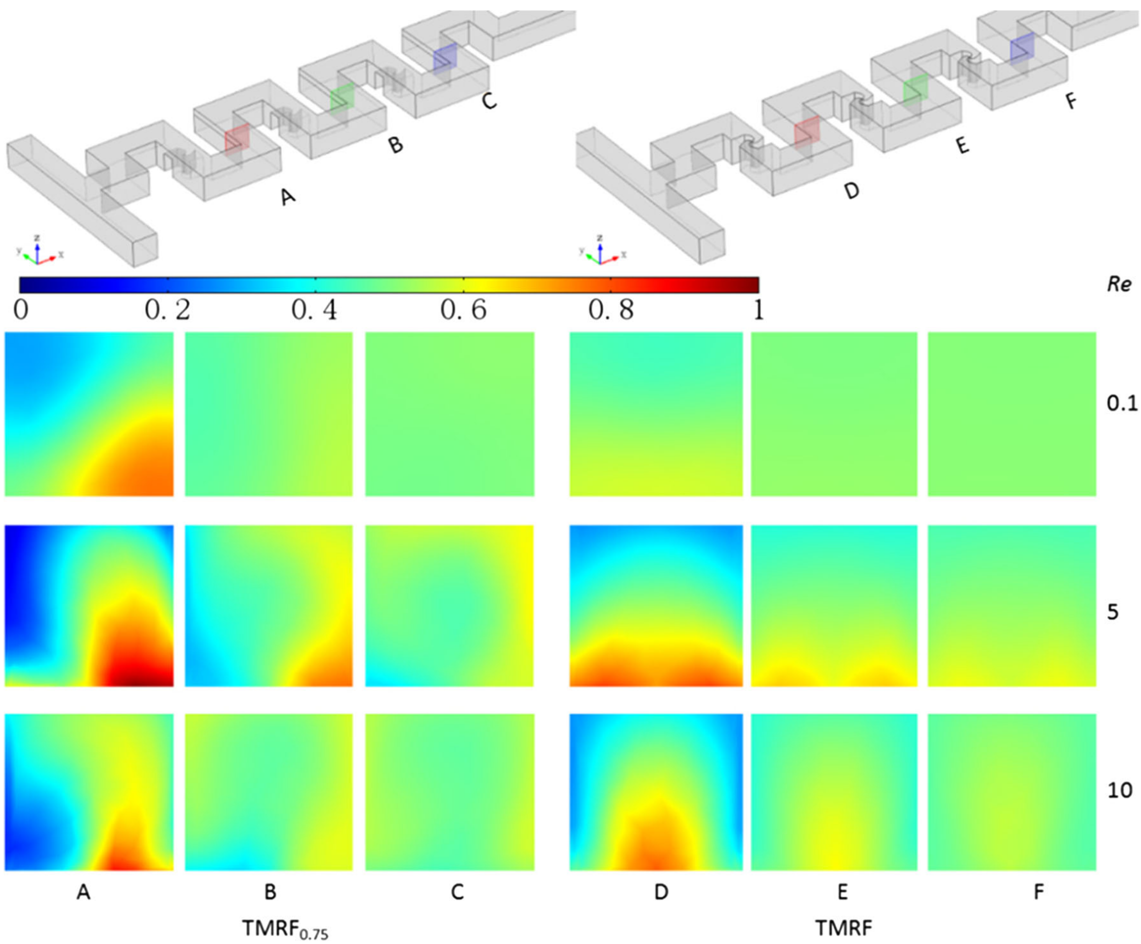

Fig. 19 Concentration distribution of unit planes of $TMRF_{0.75}$ and TMRF at *Re* of 0.1, 5 and 10

in the square-wave micromixer at a *Re* of 50, because the reversed turn indeed enhanced the centrifugal force at the turn and produced secondary flow to enhance mixing. By comparing velocity-vector plots on planes of TMRF and the square-wave micromixer at various *Re*, the intensity of the secondary flow of TMRF was stronger than the square-wave micromixer's at each *Re*.

(iv) By comparing $TMRF_X$, namely TMRF, $TMRF_{0.75}$, $TMRF_{0.5}$, $TMRF_{0.25}$, it can be concluded that when X (h/H) of $TMRF_X$ is small, the reversed turn doesn't enhance mixing obviously, especially $TMRF_{0.25}$. At most *Re*, the mixing performance of $TMRF_X$ became better with the X (h/H) of $TMRF_X$ increasing.

(v) Because the obstacle in $TMRF_{0.75}$ is not in direct contact with the upper surface of $TMRF_{0.75}$ and some fluid rushes through the space left behind. The other fluid flows along the reversed turn and joins the fluid over the reversed turn. Therefore a vortex forms on account of centrifugal force before the right-angled bend but it doesn't happen in TMRF. So at most *Re*, the mixing performance of $TMRF_{0.75}$ is similar to TMRF's, even beyond. What's more, TMRF has a larger pressure drop than $TMRF_{0.75}$, which means that TMRF have taken more energy than $TMRF_{0.75}$. For a wide range of *Re* ($Re \leq 0.1$ or $Re \geq 10$), $TMRF_{0.75}$ delivers a great performance and the mixing efficiency was greater than 95 %. Even in the range of 0.1–10 for the *Re*, the mixing efficiency of $TMRF_{0.75}$ is greater than 85 %.

Acknowledgments This work was supported by National Natural Science Foundation of China (51405214), Liaoning Province Doctor Startup Fund (20141131), Fund of Liaoning Province Education Administration (L2014241), and the Fund in Liaoning University of Technology (X201301).

References

N Aage, T H Poulsen, A Gersborg-Hansen, et al. Topology optimization of large scale stokes flow problems[J]. Struct. Multidiscip. Optim., **35**(2): 175–180 (2008)

M Abdelwahed, M Hassine, Topological optimization method for a geometric control problem in stokes flow[J]. Appl. Numer. Math., **59**(8): 1823–1838 (2009)

C S Andreasen, A R Gersborg, O Sigmund, Topology optimization of microfluidic mixers[J]. Int. J. Numer. Methods Fluids, **61**(5): 498–513 (2009)

M A Ansari, K Y Kim, Mixing performance of unbalanced split and recombine micomixers with circular and rhombic sub-channels[J]. Chem. Eng. J., **162**(2): 760–767 (2009)

N Aoki, R Umei, A Yoshida, et al. Design method for micromixers considering influence of channel confluence and bend on diffusion length[J]. Chem. Eng. J., **167**(2): 643–650 (2011)

T Borrvall, J Petersson, Topology optimization of fluids in stokes flow[J]. Int. J. Numer. Methods Fluids, **41**(1): 77–107 (2003)

A Cantu-Perez, S Barrass, A Gavriilidis, Residence time distributions in microchannels: comparison between channels with herringbone structures and a rectangular channel[J]. Chem. Eng. J., **160**(3): 834–844 (2010)

V J Challis, J K Guest, Level set topology optimization of fluids in stokes flow[J]. Int. J. Numer. Methods Eng., **79**(10): 1284–1308 (2009)

X Chen, Topology optimization of microfluidics—a review[J]. Microchem. J., **127**: 52–61 (2006)

X Chen, Z Zhang, D Yi, et al. Numerical studies on different two-dimensional micromixers basing on a fractal-like tree network[J]. Microsyst. Technol., 1-9 (2015)

X Chen, T Li, H Zeng, et al. Numerical and experimental investigation on micromixers with serpentine microchannels[J]. Int. J. Heat Mass Transf., 98: 131–140 (2016)

Y Deng, Z Liu, P Zhang, et al. A flexible layout design method for passive micromixers[J]. Biomed. Microdevices, **14**(5): 929–945 (2012)

Y Deng, Z Liu, Y Wu,. Topology optimization of steady and unsteady incompressible Navier–stokes flows driven by body forces[J]. Struct. Multidiscip. Optim., **47**(4): 555–570 (2013)

X B Duan, Y C Ma, R Zhang, Shape-topology optimization for Navier–stokes problem using variational level set method[J]. J. Comput. Appl. Math., **222**(2): 487–499 (2008)

A Evgrafov, Topology optimization of slightly compressible fluids[J]. ZAMM-Journal of Applied Mathematics and Mechanics/Zeitschrift für Angewandte Mathematik und Mechanik, **86**(1): 46–62 (2006)

A Gersborg-Hansen, O Sigmund, R B Haber, Topology optimization of channel flow problems[J]. Struct. Multidiscip. Optim., **30**(3): 181–192 (2005)

J K Guest, J H Prévost, Topology optimization of creeping fluid flows using a Darcy–stokes finite element[J]. Int. J. Numer. Methods Eng., **66**(3): 461–484 (2006a)

J K Guest, J H Prévost, Topology optimization of creeping fluid flows using a Darcy–stokes finite element[J]. Int. J. Numer. Methods Eng., **66**(3): 461–484 (2006b)

J K Guest, J H Prévost, Design of maximum permeability material structures[J]. Comput. Methods Appl. Mech. Eng., **196**(4): 1006–1017 (2007)

S Hossain, M A Ansari, K Y Kim, Evaluation of the mixing performance of three passive micromixers[J]. Chem. Eng. J., **150**(2): 492–501 (2009)

S Kreissl, G Pingen, K Maute, Topology optimization for unsteady flow[J]. Int. J. Numer. Methods Eng., **87**(13): 1229–1253 (2011)

Y Lin, Numerical characterization of simple three-dimensional chaotic micromixers[J]. Chem. Eng. J., **277**: 303–311 (2015)

L H Olesen, F Okkels, H Bruus, A high-level programming-language implementation of topology optimization applied to steady-state Navier–Stokes flow[J]. arXiv preprint physics/0410086, (2004)

R L Panton, Incompressible flow[J]. (1984)

G. Pingen, K. Maute, Optimal design for non-Newtonian flows using a topology optimization approach[J]. Computers & Mathematics with Applications **59**(7), 2340–2350 (2010)

E Saatdjian, A J S Rodrigo, J P B Mota, On chaotic advection in a static mixer[J]. Chem. Eng. J., **187**: 289–298 (2012)

K Svanberg, The method of moving asymptotes—a new method for structural optimization[J]. Int. J. Numer. Methods Eng., **24**(2): 359–373 (1987)

N Wiker, A Klarbring, T Borrvall, Topology optimization of regions of Darcy and stokes flow[J]. Int. J. Numer. Methods Eng., **69**(7): 1374–1404 (2007)

S Zhou, Q Li, A variational level set method for the topology optimization of steady-state Navier–stokes flow[J]. J. Comput. Phys., **227**(24): 10178–10195 (2008)

T Zhou, Y Xu, Z Liu, et al. An enhanced one-layer passive microfluidic mixer with an optimized lateral structure with the dean effect[J]. J. Fluids Eng., **137**(9): 091102 (2015)